Prograde Rayleigh wave particle motion

Toshiro Tanimoto, Luis Rivera

Geophys. J. Int. (2005) **162,** 399–405 doi: 10.1111/j.1365-246X.2005.02481.x

Prograde Rayleigh wave particle motion

T. Tanimoto[1] and L. Rivera[2]

[1] *Institute for Crustal Studies and Department of Geological Sciences, University of California, Santa Barbara, California* 93106, *USA. E-mail: toshiro@geol.ucsb.edu*

[2] *EOST-IPGS, 5 rue Rene Descartes,* F67084 *Strasbourg Cedex, France*

Accepted 2004 September 24. Received 2004 July 20

SUMMARY

Fundamental mode Rayleigh waves generally show retrograde particle motion at the surface of the Earth. If there exists a thick sedimentary layer, however, reversal of the sign of vertical eigenfunction occurs near the surface, resulting in prograde Rayleigh-wave particle motion at the surface. We show that, for structures similar to those found in the Los Angeles basin (with thickness up to 8 km), surface prograde motion may occur within the frequency band 0.05–0.3 Hz. Although it has been suggested that the effect of gravity on waves in unconsolidated surface layer may be important, partitioning of energy between the elatic and gravitational energy shows that the gravitational energy is less than 1 per cent and thus is not important. The phenomenon is caused by elastic effects, mainly caused by extremely slow shallow seismic velocities. Observation of prograde elliptical particle motion may be difficult, however, because particle motion is largely horizontal and high microseismic noise exists in the same frequency band.

Key words: particle motion, prograde, Rayleigh waves, sediment.

1 INTRODUCTION

Particle motion for fundamental mode Rayleigh waves is elliptical and is generally believed to be retrograde at the surface. Many textbooks in seismology discuss this important feature in Rayleigh waves using a uniform half-space model as an example (e.g. Shearer 1999). In the case of uniform elastic half-space model, this is rigorously correct for Rayleigh waves. In a more realistic layered earth model, at least to our knowledge, it is not known whether Rayleigh waves always possess retrograde particle motion at the surface.

One of the main purposes of this paper is to show some concrete examples of prograde surface particle motion of Rayleigh waves. We will demonstrate this point by using structure which mimic seismic structure in the Los Angeles basin; in this paper, unless otherwise noted, a sedimentary layer is not a homogeneous layer but is a layer with linear gradient for density and elastic velocities. We will show that prograde motion can result if surface seismic velocities are as low as 400 m s^{-1} for *P* waves and 200 m s^{-1} for *S* waves, typical numbers often found in basin structures.

After introduction of our convention and seismic velocity models in Section 2, we will show our main numerical results in Section 3 and discuss some aspects of our results in Section 4.

2 CONVENTION AND SEISMIC MODEL

We use a spherical earth model with radius R and include effects of gravity in the calculations (e.g. Takeuchi & Saito 1972; Aki & Richards 1980; Dahlen & Tromp 1998). Our convention for eigenfunctions of a spheroidal mode (Rayleigh waves) is given by

$$(u_r, u_\theta, u_\phi) = \left(U(r) Y_l^m(\theta, \phi), V(r) \frac{\partial Y_l^m}{\partial \theta}, V(r) \frac{1}{\sin\theta} \frac{\partial Y_l^m}{\partial \phi} \right), \quad (1)$$

where displacements in the radial, co-latitudinal, and longitudinal directions are denoted by u_r, u_θ and u_ϕ, respectively, $U(r)$ is the vertical eigenfunction, $V(r)$ is the horizontal eigenfunction and Y_l^m is the spherical harmonics with angular degree l and azimuthal order m. For the definition of $V(r)$, we follow the convention of Takeuchi & Saito (1972).

We consider seismic models that have a shallow sedimentary layer with linear velocity and density gradient. Below this layer, the crust and mantle are assumed to have constant velocities and densities. Motivation for adoption of such a model is from seismic structures in the Los Angeles Basin; Fig. 1 shows velocity models near two stations, USC (University of Southern California) and WTT (Watts), from the Community Velocity Model 3.0 of the Southern California Earthquake Center (Magistrale *et al.* 2000; Kohler *et al.* 2003). The figures suggest that both structures can be approximated well by linear gradient in the sedimentary layer (about 6 km at USC and 8–9 km at Watts) and constant crustal velocities below.

Three examples of our models are shown in Fig. 2; the left is the limiting case of no sedimentary layer, the middle is with a sedimentary layer of thickness 4 km and the right is with a sedimentary layer with thickness 8 km. In all these models, surface values are $\alpha_0 = 0.405$ km s^{-1} (*P*-wave velocity), $\beta_0 = 0.185$ km s^{-1} (*S*-wave velocity) and $\rho_0 = 1.5$ g cc^{-1} (density), crustal values are 6.5 km s^{-1} (α_c), 3.6 km s^{-1} (β_c) and 2.85 g cc^{-1} (ρ_c) and mantle values are 7.8 km s^{-1} (α_m), 4.5 km s^{-1} (β_m) and 3.3 g cc^{-1} (ρ_m). Within

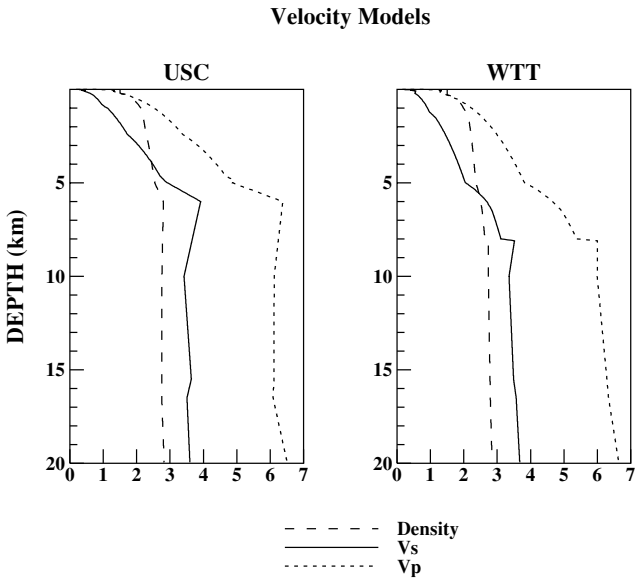

Figure 1. Two examples of seismic structure from the Los Angeles Basin. SCEC Community Velocity Model 3.0 was used to construct these models near USC and WTT. Computer program for the SCEC models are available from the SCEC website www.scec.org. Unit for density is g cm^{-3} and unit for velocities are km s^{-1}.

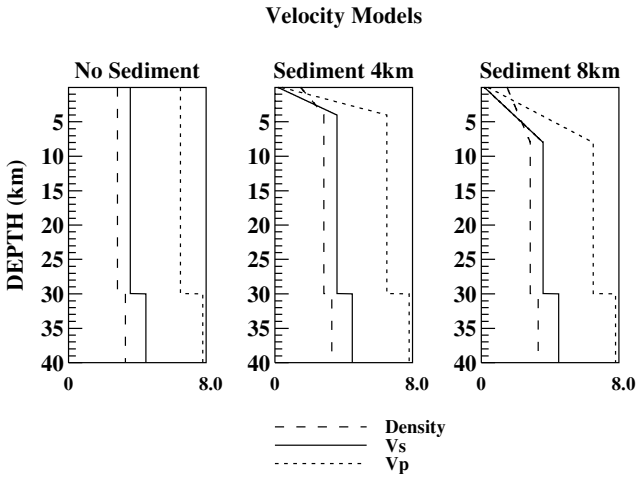

Figure 2. Seismic models in this paper contain a sedimentary layer, a homogenous crust and a homogenous mantle which starts at depth 30 km. Linear gradient is assumed within the sedimentary layer. The limiting case of no sedimentary layer (left), an example with 4-km thick sediment (middle) and another example with 8-km thick sediment (right) are shown. Detailed numbers for these models are given in the text. Unit for density is g cm^{-3} and unit for velocities are km s^{-1}.

the top sedimentary layer, the surface values and the crustal values are linearly interpolated over the thickness of the layer (H).

Eigenfunctions for the case without the sedimentary layer (Fig. 2, left) are shown in Fig. 3 at four selected frequencies from 0.1 to 0.25 Hz. They have well-known shape of $V(r)$ and $U(r)$ in that $V(r)$ has one zero-crossing point and $U(r)$ is positive throughout the medium. Existence of a sedimentary layer modifies near-surface behaviour of $U(r)$ greatly, resulting in negative values of $U(R)$ under certain conditions (therefore one zero-crossing). The horizontal eigenfunction $V(r)$ maintains one zero-crossing in all cases of our discussion below. We take a convention that $V(R)$ is negative in this paper.

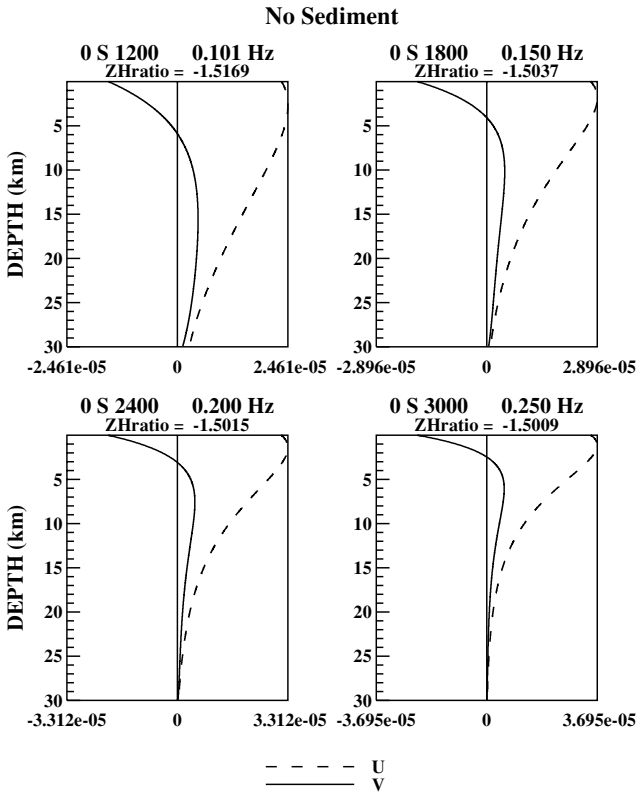

Figure 3. Eigenfunctions for the case without the sedimentary layer (Fig. 2, left) are shown at 0.1, 0.15, 0.2 and 0.25 Hz. The ZH-ratios are given at the top of each mode. They have 'typical' well-known shape for U and V.

Ratios of the surface displacements, $U(R)$ to $(l+0.5)\ V(R)$, are termed as the ZH-ratio in this paper and are given at top of each panel in Fig. 2. Since the model is close to a uniform half-space, this ratio is almost constant and is about -1.5. Slight frequency dependence of the ZH-ratio arises from differences between the crust and mantle structure, because longer period modes start to sense the mantle structure below.

In the epicentral coordinates and in asymptotic distance ranges, we can write the out-going Rayleigh-wave displacement field as (our Fourier convention assumes $e^{i\omega t}$ on the right-hand side)

$$u_r = U(r)Y_l^m \propto U(r)e^{-i(l+0.5)\theta} \tag{2}$$

$$u_\theta = V(r)\frac{\partial Y_l^m}{\partial \theta} \propto -i(l+0.5)V(r)e^{-i(l+0.5)\theta}, \tag{3}$$

where we dropped the common amplitude and phase factors in the last terms. Near the surface where the signs of U and V differ (as in Fig. 2), phase shift between u_θ and u_r is given by i (or $e^{i\frac{\pi}{2}}$) and there is a $\pi/2$ phase advance of u_θ with respect to u_r. This indicates the well-known retrograde particle motion. Below the zero-crossing depth of $V(r)$, U and V have the same sign and thus the prograde particle motion results beyond this depth.

What we examine below is essentially how these features will be modified by the effects of sedimentary layers.

3 NUMERICAL INVESTIGATIONS

3.1 Two examples

We begin by showing two examples of eigenfunctions and their ZH ratios; the first model has a 4-km thick sedimentary layer (Fig. 2,

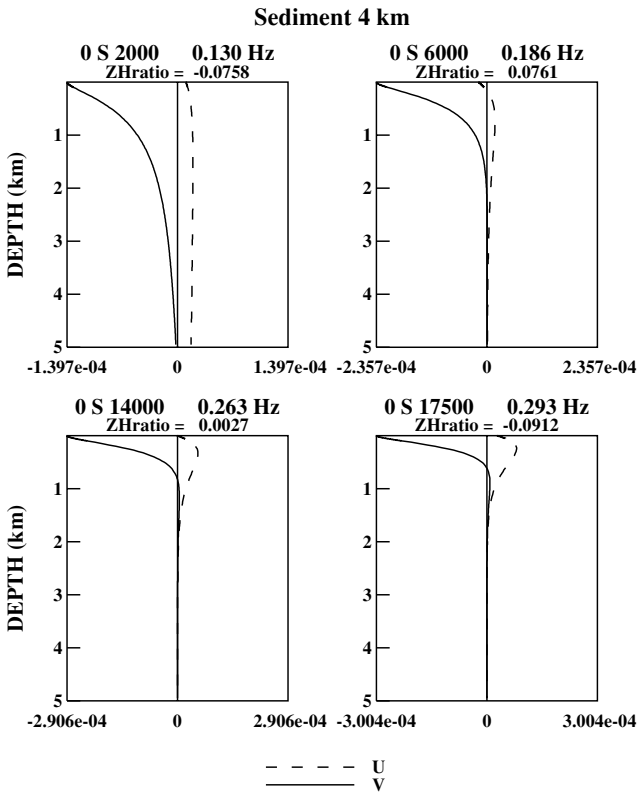

Figure 4. Four selected modes for the model with 4-km thick sedimentary layer. Surface values for the vertical eigenfunctions for ${}_0S_{6000}$ and ${}_0S_{14000}$ are negative. Reversal of the sign of U near the surface creates a depth range for prograde particle motion at shallow depths.

middle) and the second model has a 8-km thick sedimentary layer (Fig. 2, right).

Fig. 4 shows four selected modes for the case of 4-km sedimentary layer. Comparison against the eigenfunctions in the uniform crust (Fig. 3) indicates two main differences; the first is the overall low amplitudes for the vertical eigenfunctions $U(r)$. Note that, in Fig. 3, the maximum value in $U(r)$ and $V(r)$ is attained by the maximum of $U(r)$ close to the surface, whereas the maximum in Fig. 4 is attained by the surface values of V. This should be related to low seismic velocity at shallow depths in the 4-km sediment model.

The second difference, which is central to our discussion, is the rapid decrease of amplitudes of $U(r)$ very close to the surface. In fact, the sign of $U(R)$ becomes negative for some frequency range. Note that the ZH-ratios for ${}_0S_{6000}$ (0.186 Hz) and ${}_0S_{14000}$ (0.263 Hz) are positive, indicating $U(R)$ is negative for both modes. Fig. 5 shows the frequency dependence of the ZH-ratios for frequencies between 0.1 and 0.3 Hz. It is clear from this figure that reversal of the sign of $U(R)$ (thus reversal of the ZH-ratios) occurs between about 0.14 and 0.26 Hz for this 4-km sedimentary layer model. Locations of four modes in Fig. 4 were selected from different regimes of particle motion and are indicated by solid circles.

Figs 6 and 7 show similar results for the case of 8-km thick sedimentary layer. Overall qualitative features are the same with the case of 4-km model, except that the reversal of the sign of $U(R)$ occurs at a lower frequency range; Fig. 7 shows that this reversal occurs between about 0.07 and 0.13 Hz for this model. Eigenfunctions in Fig. 6 confirm that surface values of U become negative in this frequency range. The modes were selected again from different regimes of particle motion; they have quite different angular

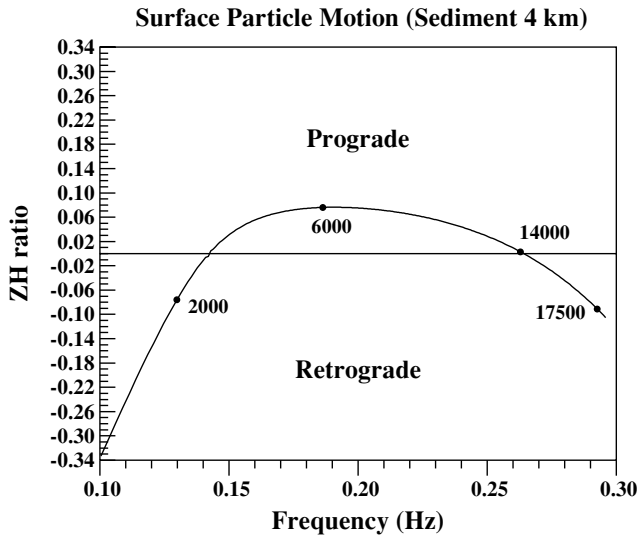

Figure 5. The ZH-ratio $U(R)/(l + 0.5)V(R)$ as a function of frequency. Reversal of the sign occurs for frequencies between 0.14 and 0.26 Hz. Four circles indicate the modes in Fig. 4.

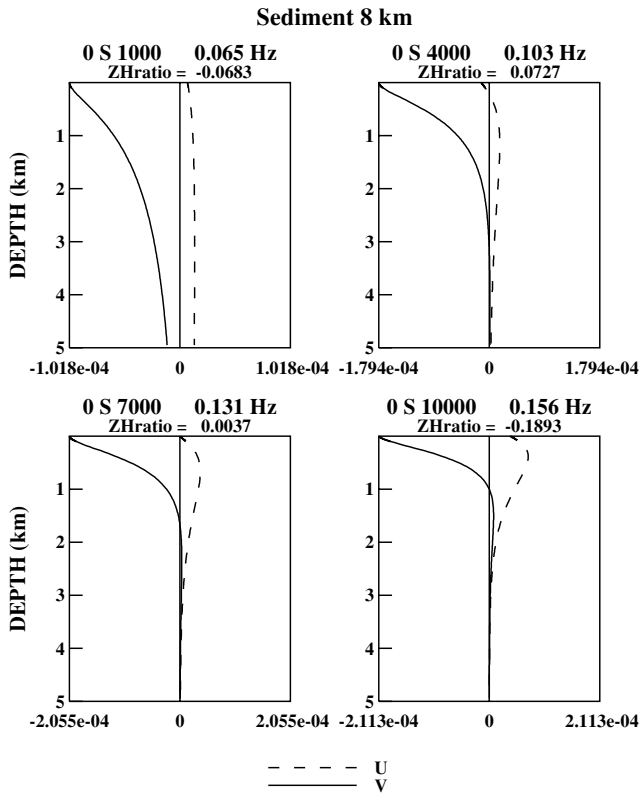

Figure 6. Same with Fig. 4 except that this is for the 8-km thick sediment model.

degrees from those selected in Fig. 5 because of differences in the underlying seismic velocity structure.

3.2 Summary of results and scaling

Summary of similar calculations for various thickness of sedimentary layer is shown in Fig. 8; the minimum thickness is 0.1 km, which

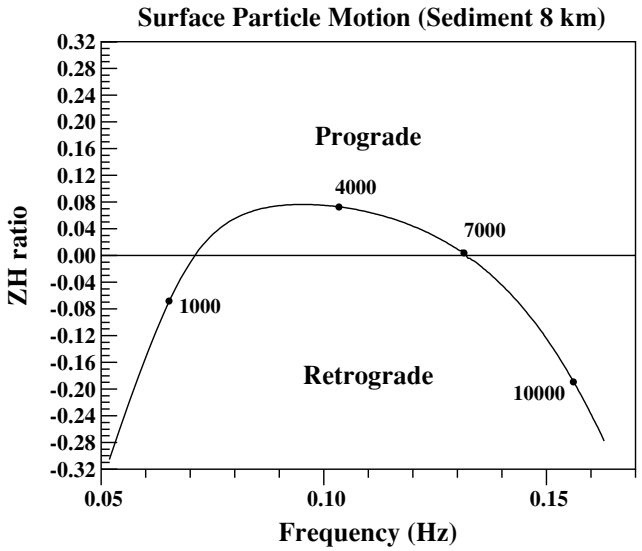

Figure 7. Same with Fig. 5 except that this is for the 8-km thick sediment model. Sign reversal occurs at a lower frequency range, approximately between 0.07 and 0.13 Hz.

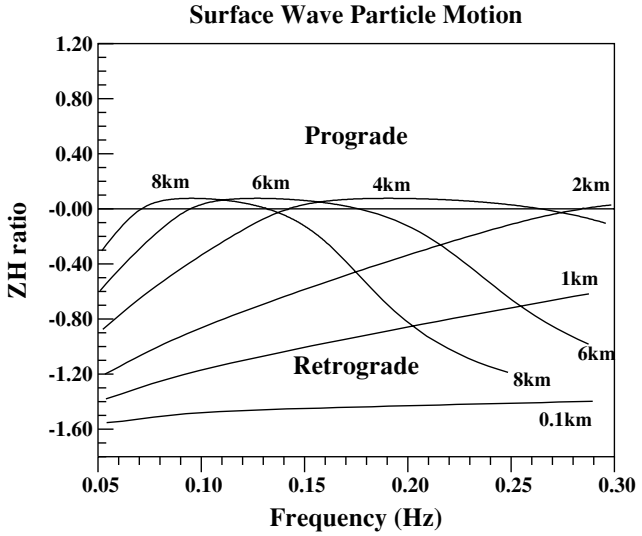

Figure 8. Summary of ZH-ratio versus frequency plot for models with different thickness of sedimentary layer. Thickness is varied from 0.1 to 8 km. For each model, the ZH-ratio increases with frequency from low-frequency end, reaches its maximum (in the positive range) and decreases for higher frequencies. The frequency range of the peak moves toward lower frequencies with increasing thickness of sedimentary layer.

gives similar results to the uniform crustal model and the maximum thickness is 8 km. We used the same surface seismic parameters, the crustal parameters and the mantle parameters in all cases. The only difference among these models is the thickness of the sedimentalry layer, in which linear changes in density and seismic velocities are assumed.

Qualitatively, similar features are found in all curves in Fig. 8. In general, a ZH-ratio increases with frequency from the low-frequency end, reaches its maximum in the slightly positive range and decreases for higher frequencies. The main difference is seen in the frequency range of the sign reversal or the location of the maximum in each curve; the general trend is that the thicker the sediments, the lower this frequency range of sign reversal.

The maximum value of each curve (ZH ratio) in Fig. 8 is the same, approximately 0.076, although the maximums are only seen for three models, the 8-km, the 6-km and the 4-km models within the frequency band 0.05–0.3 Hz. In addition, the peak frequency for the 8-km model is almost exactly half of the peak frequency for the 4-km model; there is actually a scaling relation among these curves, because we have essentially a sedimentary layer with thickness (H) over a uniform half-space (underlying crust). Strictly speaking, there is mantle from the depth 30 km, but since eigenfunctions of these high-frequency modes essentially lose amplitudes within the crust before reaching the mantle, the crust can be regarded as a uniform half-space. In such a case, there is only one scaling length in the model—thickness of the sedimentary layer H. If we halve the thickness of sediment, say from 8 to 4 km, we can simply halve the wavelength and double the frequency axis to get the eigenfunctions and eigenfrequencies; the overall shape of the curve of the ZH ratios remains the same. One can then imagine a generic curve such as the one shown in the top panel of Fig. 9. If we define this shape by a function $F()$, we should be able to write

$$F(\omega H) = -\frac{U}{(l+0.5)V}, \tag{4}$$

where ω is the angular frequency and the right-hand side is the ZH ratio. If we halve H and double ω, the value of the function $F()$ remains the same obviously.

If the crust has more layers, such a scaling does not work in an exact manner as we see in Fig. 8.

3.3 Existence of the maximum in the ZH ratio

One of the most fundamental questions we can ask in Fig. 9 is, why is there a maximum, first of all, in a model with a sedimentary layer?

This is most likely related to S-wave velocity structure within the sediment. In Fig. 9, both in the top and bottom panels, an arrow indicates the frequency that corresponds to the round-trip S-wave traveltimes within the sedimentary layer. This frequency is not exactly at the maximum, perhaps because we are dealng with Rayleigh waves that have some effects from P-wave and density structure. But the frequency approximately matches the maximum of the ZH ratio. The bottom panel shows that it also matches the minimum of the vertical eigenfunction and the maximum of absolute value of the horizontal eigenfunction. In other words, approximately at the resonant frequency of S waves within a sedimentary layer, U becomes minimum and $|V|$ becomes maximum, making Rayleigh waves dominated by shear motion. We postulate therefore that the existence of this maximum region in the ZH ratio is related to a resonance condition of the sedimentary layer.

3.4 Prograde motion within the top thin layer

Reversal of the sign of $U(r)$ close to the surface has interesting implications as to the observations of particle motion; it means that, at least for some finite frequency intervals, surface particle motion of Rayleigh waves can be prograde if there is a thick sedimentary layer. If this happens, instead of having two depth ranges for Rayleigh wave particle motions (a normal case in which retrograde motion is found at shallow depths and prograde motion is found below the zero-crossing depth of the horizontal eigenfunction), there are three different depth ranges; the prograde particle motion within

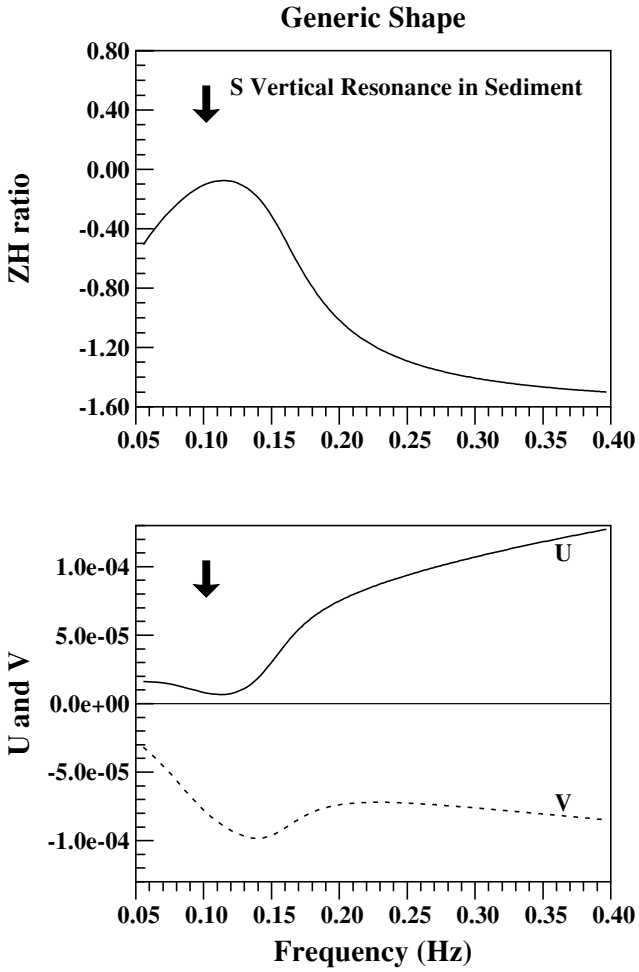

Figure 9. Generic shape of the ZH ratio. There is scaling because the underlying crust is essentially a halfspace for high-frequency modes in our model. Thickness of sediment becomes the only scaling length. The maximum region is closely related to the resonant frequency of *S* waves in the sediment. Near this frequency, Rayleigh waves are dominated by shear motion in that U reaches the minimum and the absolute value of V reaches a maximum. It may appear the ZH-ratio reaches the maximum but in terms of the absolute numbers, it reaches the minimum.

the shallowest depth range (where both $U(r)$ and $V(r)$ are negative), the retrograde particle motion at intermediate depths (where $U(r)$ is positive and $V(r)$ is negative), and the prograde particle motion at depths where both $U(r)$ and $V(r)$ are positive.

3.5 Effect of shallow velocity

Numerical computations summarized in Fig. 8 have been performed with fixed surface seismic velocities, found in the SCEC model ($\alpha_0 = 0.405$ km s^{-1}, $\beta_0 = 0.185$ km s^{-1}). In order to see the effects caused by variations of these velocities, we performed similar computations for models with higher surface seismic velocities. Specifically, we show results of three models; the first with twice the values of α_0 and β_0 at the surface (model 2), the second with three times the values of α_0 and β_0 (model 3) and the third with five times the values of α_0 and β_0 (model 5). We kept the thickness of sedimentary layer at 6 km in all cases and used the same crustal and mantle values. For density, we used $\rho = 1.5$ (g cc^{-1}) for the original

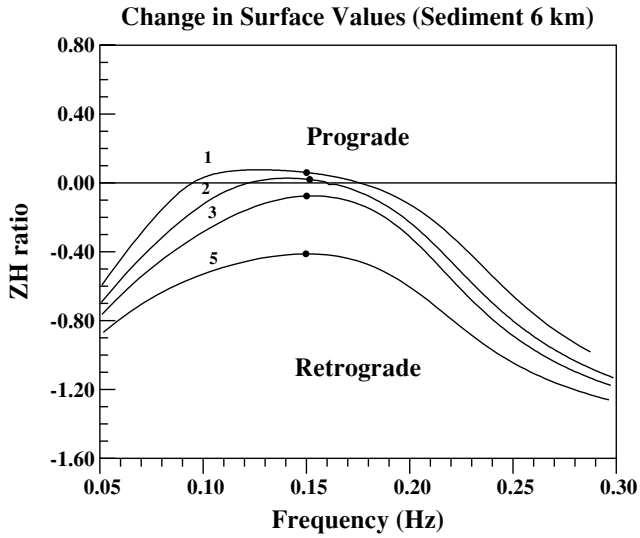

Figure 10. Effects of surface seismic velocities. Curve 1 is the same with the models in Fig. 2 except that we used 6 km for the thickness. Curves 2, 3 and 5 indicate that the surface values were multiplied by 2, 3 and 5 respectively in comparison to the original model 1. All cases show the maximum between 0.1 and 0.2 Hz, but the maximum values do not reach positive region for the models 3 and 5. Surface seismic velocities must be extremely low to have positive ZH-ratios or have prograde particle motion at the surface.

model and $\rho = 2.0$ (g cc^{-1}) for models 2, 3 and 5. Density does not change the main qualitative features in the following results.

Results for the ZH-ratio as functions of frequencies are shown in Fig. 10. The numbers by each curve, 1 to 5, indicate the multiplication factors to α_0 and β_0 for surface values in each model. All curves basically show existence of the maximum region between about 0.1 and 0.2 Hz. The most critical point in this figure is that the maximum values of the ZH-ratio do not become positive for models 3 and 5.

Eigenfunctions at selected points on each curve (solid circles in Fig. 7a), at about 0.15 Hz, are shown in Fig. 11. They show clearly that vertical eigenfunctions $U(r)$ for models 1 and 2 reverse their sign near the surface but those for models 3 and 5 do not. The transition occurs when the surface seismic velocities are 2.41 times the values in the original model (Fig. 2). In unit of velocity, the surface *P*-wave velocity is 0.975 km s^{-1} and *S*-wave velocity is 0.445 km s^{-1} for density of 2 g cc^{-1}.

It is clear from Fig. 10 that reversal of the sign in $U(r)$ near the surface (and the existence of the prograde surface particle motions) requires existence of extremely slow seismic velocities near the surface. In fact, *S*-wave velocity in unconsolidated layer can be as low as 10–100 (m s^{-1}) (e.g. Chavéz-García *et al.* 1995), smaller than the numbers we used for calculations. It seems quite reasonable to expect that the reversal of particle motion may be occurring in some sedimentary basins.

4 DISCUSSION

4.1 Effect of gravity

Gilbert (1967) analysed effects of gravity on elastic waves in a uniform half-space. Specifically, he analysed the effect of gravity on the Rayleigh pulse ($\bar{S}$) and the leaking mode pulse ($\bar{P}$); the former has the retrograde particle motion and the latter has the

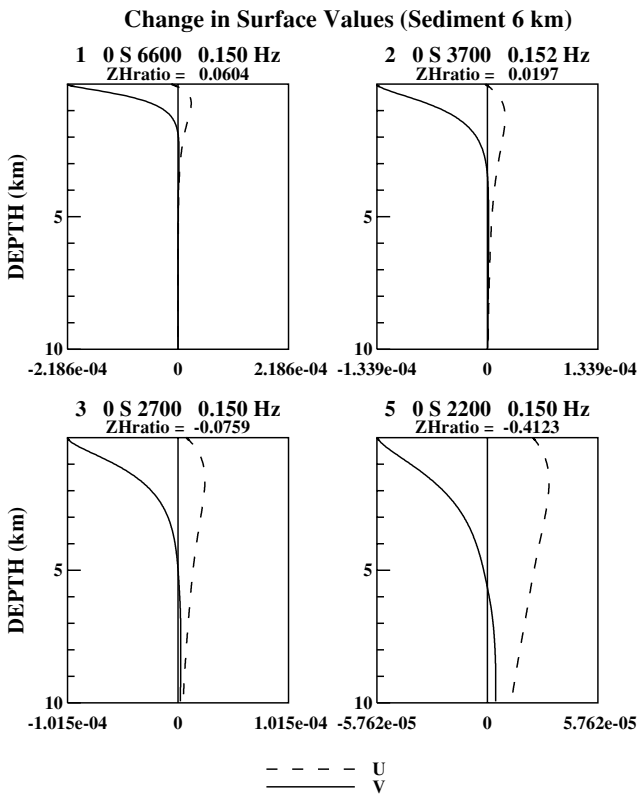

Figure 11. Eigenfunctions for four selected modes in Fig. 10. Note that the surface values of U are negative for models 1 and 2 but are positive for 3 and 5.

prograde particle motion. He showed that, in the presence of gravity, as S-wave velocity decreases, the $\bar{S}$ pulse becomes insignificant and the $\bar{P}$ pulse approaches the behaviour of the classical gravity waves (for example, ocean waves).

There are subsequent studies that claimed observation of such gravity waves after the 1985 Mexico earthquake in a sedimentary basin (e.g., Lomnitz 1990), although the claim by Lomnitz (1990) was discredited by Chávez-Garćia & Bard (1993a,b). Motivated by these studies, we examined the effects of gravity on Rayleigh waves in the frequency range of our discussion (0.05–0.3 Hz).

We stress, however, that the main subject of this paper is quite different from Chávez-García & Bard (1993a,b); the range of the Poisson's ratio in this study (less than 0.4) is entirely different from those used in Chávez-García & Bard (1993a,b) (or Lomnitz 1990) who used values close to 0.5 (or 0.499 999). Their main point in modelling focused on fluid-like behaviour of sediments. Also our normal mode analysis is different from a technique in Chávez-García & Bard (1993a) who approximated the effects of gravity by modifying surface boundary conditions.

We directly evaluated various types of potential energy, partitioned for elastic (bulk and shear) and gravitational energy. Equipartition of energy between the kinetic and potential energy gives (Dahlen & Tromp 1998)

$$T = E_\kappa + E_\mu + E_g, \tag{5}$$

where T is the kinetic energy given by

$$T = \omega^2 \int_0^R \rho\{U^2 + l(l+1)V^2\} r^2\, dr \tag{6}$$

and E_κ, E_μ and E_g are elastic potential energy related to bulk, elastic potential energy for shear and gravitational potential energy. In our notation, they are

$$E_\kappa = \int_0^R \kappa \left\{ r\frac{dU}{dr} + 2U - l(l+1)V \right\}^2 dr \tag{7}$$

$$E_\mu = \int_0^R \mu \left[\frac{1}{3} \left\{ 2r\frac{dU}{dr} - 2U + l(l+1)V \right\}^2 + l(l+1)\left(r\frac{dV}{dr} - V + U \right)^2 + \frac{(l+2)!}{(l-2)!} V^2 \right] dr \tag{8}$$

$$E_g = \int_0^R \rho \left[U\frac{dP}{dr} + \frac{l(l+1)}{r} VP + 4\pi G\rho U^2 - \frac{2g}{r} U\{2U - l(l+1)V\} \right] r^2\, dr, \tag{9}$$

where R is the radius of the Earth, P is the gravitaional potential perturbation, G is the gravitational constant and g is the gravitational acceleration. We define the fractional energy by $f_\kappa = E_\kappa/T$, $f_\mu = E_\mu/T$, $f_g = E_g/T$. While a term can become negative, the sum of the three terms $E_\kappa + E_\mu + E_g$ is always positive.

In Table 1, we list f_κ, f_μ, and f_g for selected modes from 0.05 to 0.3 Hz. The model has a 4-km sedimentary layer. This table shows that the gravitational potential energy is always very small (less than 1 per cent) in comparison to elastic potential energy for all modes under consideration. This is true even when the surface value of the vertical eigenfunction changes its sign. We therefore conclude that the effect of gravity is not important in our case, even though the surface S-wave velocity is as small as 200 (m s^{-1}).

In an alternative check on this result, we computed the ZH-ratios by two other methods; the first by a code for flat-layer media (Herrman 1978) and the second by a code for spherical media without gravity effects (Saito 1988). Fig. 12 shows the comparison of three methods and a close match among different methods. The match between the flat-layer code and the spherical code without gravity is extremely good; in fact, the two curves virtually overlap in Fig. 12. There exists a small but systematic shift of the case with gravity effects at higher frequencies, somewhat to our surprise, but the gravitational energy calculations also indicate an increasing trend (at least within 0.1–0.3 Hz) and thus this systematic shift is consistent with energy calculations. (This cannot continue for higher frequencies, however, because effect of gravity is generally less important at higher frequencies.) Overall, these results support that the shape of eigenfunctions are determined by elasticity, including the reversal of the vertical eigenfunction near the surface; it should perhaps be stressed that prograde particle motions are confirmed by codes that do not take into account effects of gravity.

Poisson's ratios in our seismic models vary within 0.25–0.37. They are much smaller than the values used for arguments of

Table 1. Partition of potential energy (sediment thickness 4 km).

Frequency (Hz)	Mode	Bulk (f_κ)	Shear (f_μ)	Gravitational (f_g)
0.10	${}_0S_{1350}$	0.188	0.813	−0.001
0.15	${}_0S_{3000}$	0.190	0.811	−0.001
0.20	${}_0S_{7300}$	0.230	0.771	−0.001
0.25	${}_0S_{12600}$	0.299	0.703	−0.002
0.30	${}_0S_{18400}$	0.370	0.634	−0.004

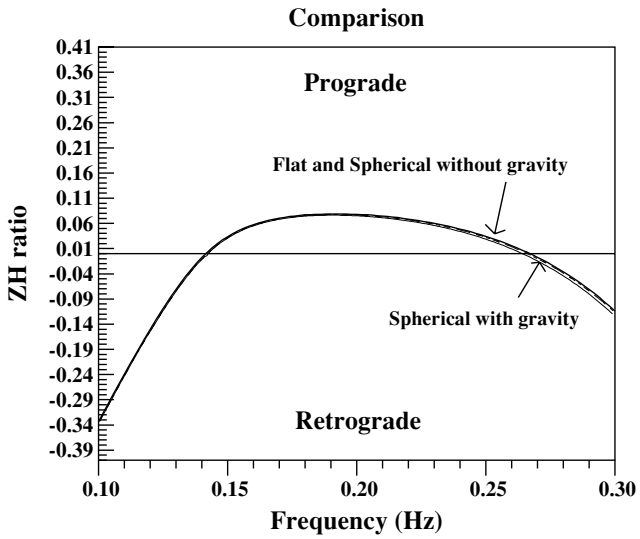

Figure 12. Comparison of the ZH-ratios computed by three methods: a code for flat-layered medium, a code for spherical medium without effect of gravity and a code for a spherical medium with gravity. Results for the flat-layered medium and for the spherical case without gravity overlaps almost completely. Spherical results with gravity effects deviate slightly at higher frequency end, surprisingly, but this is consistent with our energy calculation in Table 1. Overall, the match among different methods is excellent and support that elasticity causes the prograde motion at the surface.

existence of gravity waves in unconsolidated sedimentary structures, typically very close to 0.5. Therefore, our results do not deny or support the claim of gravity-wave observation after the 1985 Mexico earthquake. We have simply shown examples of prograde Rayleigh-wave motion within elastic media, typically found in basin structures.

4.2 Implication for observation

For a realistic sedimentary-basin structure, we showed that prograde particle motion may be occurring. But is this easy to identify in data? We point out that there are two aspects that may make this observation difficult.

The first is the existence of high microseismic noise in the frequency band of discussion. At many stations, there is ubiquitous noise (microseisms) in the band between 0.05 and 0.3 Hz. This obviously makes the observation of seismic signals difficult. It is possible, of course, that microseismic noise can be overcome if an earthquake is sufficiently large.

The second point is related to small vertical amplitude with respect to horizontal amplitude. In all cases in Fig. 8, the largest ratio was 0.074 or the horizontal amplitude is about 12–13 times larger than the vertical amplitude. Although the vertical eigenfunction reverses its sign near the surface, its surface amplitude is quite small. This is true in all of our calculations that show prograde particle motion. In fact, the motion in thick sedimentary structure is largely horizontal. Therefore, even though the motion is prograde, small vertical amplitude may make it difficult to identify it as prograde particle motion, especially in the presence of microseismic noise.

5 CONCLUSION

The major conclusion of this paper is that Rayleigh wave particle motion can become prograde near the surface, if an underlying structure has a sedimentary layer with extremely slow seismic velocities. We demonstrated this point by using fairly realistic structure that mimics seismic structure in the Los Angeles basin. Positive identification of this phenomenon may be difficult, however, because particle motion is predominantly horizontal and high microseismic noise exists in the same frequency band. It may still be possible in seismograms for large, nearby earthquakes at seismic stations in sedimentary basins.

ACKNOWLEDGMENTS

This study was performed when both of us stayed at California Institute of Technology as visiting associates. We appreciate the comments by colleagues in the Seismological Laboratory. This study was partially supported by a UCSB faculty senate grant and an NSF grant (EAR0408742) awarded to UCSB.

REFERENCES

Aki, K. & Richards, P., 1980. *Quantitative Seismology*, Freeman, New York.

Chávez-García, F.J. & Bard, P.-Y., 1993a. Gravity waves in Mexico city? – I. Gravity perturbed waves in an elastic solid, *Bull. seism. Soc. Am.,* **83,** 1637–1655.

Chávez-García, F.J. & Bard, P.-Y., 1993b. Gravity waves in Mexico city? – II. Coupling between an anelastic solid and a fluid layer, *Bull. seism. Soc. Am.,* **83,** 1656–1675.

Chávez-García, F.J., Ramos-Martinez, J. & Romero-Jimenez, E., 1995. Surface-wave dispersion analysis in Mexico city, *Bull. seism. Soc. Am.,* **85,** 1116–1126.

Dahlen, A.F. & Tromp, J., 1998. *Theoretical Global Seismology*, Princeton University Press, Princeton.

Gilbert, F., 1967. Gravitationally perturbed elastic waves, *Bull. seism. Soc. Am.,* **57,** 783–793.

Herrman, R., 1978. *Computer programs in seismology*, Vol. 2, Surface Wave Programs, Department of Earth and Atmospheric Sciences, St Louis University.

Kohler, M., Magistrale, H. & Clayton, R.W., 2003. Mantle heterogeneities and the SCEC Reference three-dimensional seismic velocity model version 3. *Bull. seism. Soc. Am.,* **93,** 757–774.

Lomnitz, C., 1990. Mexico 1985: the case for gravity waves, *Geophys. J. Int.,* **102,** 569–572.

Magistrale, H., Day, S., Clayton, R.W. & Graves, R., 2000. The SCEC southern California reference three-dimensional seismic velocity model version 2, *Bull. seism. Soc. Am.,* **90**(6B), S65–S76.

Saito, M., 1988. *Seismological Algorithms*, ed. Doornbos, D.J., Academic Press, San Diego.

Shearer, P.M., 1999. *Introduction to Seismology*, Cambridge University Press, Cambridge.

Takeuchi, H. & Saito, M., 1972. Seismic Surface Waves, in *Methods in Computational Physics,* Vol. 11, pp. 217–295, ed. Bolt, B.A., Academic Press, New York.